NASA TECHNICAL NOTE

NASA TN D-6003

FLUTTER STUDIES TO DETERMINE NACELLE AERODYNAMIC EFFECTS ON A FAN-JET TRANSPORT MODEL FOR TWO MOUNT SYSTEMS AND TWO WIND TUNNELS

by Moses G. Farmer

Langley Research Center
Hampton, Va. 23365

NATIONAL AERONAUTICS AND SPACE ADMINISTRATION • WASHINGTON, D. C. • SEPTEMBER 1970

1. Report No.	2. Government Accession No.	3.
NASA TN D-6003		

4. Title and Subtitle	5. Report Date
FLUTTER STUDIES TO DETERMINE NACELLE AERODYNAMIC EFFECTS ON A FAN-JET TRANSPORT MODEL FOR TWO MOUNT SYSTEMS AND TWO WIND TUNNELS	September 1970
	6. Performing Organization Code
7. Author(s)	8. Performing Organization Report No.
Moses G. Farmer	L-7120
	10. Work Unit No.
9. Performing Organization Name and Address	126-14-14-02
NASA Langley Research Center Hampton, Va. 23365	11. Contract or Grant No.
	13. Type of Report and Period Covered
12. Sponsoring Agency Name and Address	Technical Note
National Aeronautics and Space Administration Washington, D.C. 20546	14. Sponsoring Agency Code

15. Supplementary Notes

16. Abstract

Low-speed flutter studies of a dynamically and elastically scaled model of a large multijet transport airplane have been conducted primarily to determine the nacelle aerodynamic effects for high-bypass-ratio fan-jet engines. Data were obtained on a vertical rod mount in two wind tunnels and on a two-cable mount in one of the tunnels. The flutter response of the model was found to be dependent on nacelle aerodynamics, engine-pylon stiffness, mount-system—wind-tunnel configuration, and mass ratio.

17. Key Words (Suggested by Author(s))	18. Distribution Statement
Low-speed flutter Nacelle aerodynamics Mount-system effects Wind-tunnel effects Fan-jet transport	Unclassified – Unlimited

19. Security Classif. (of this report)	20. Security Classif. (of this page)	21. No. of Pages	22. Price*
Unclassified	Unclassified	35	$3.00

*For sale by the Clearinghouse for Federal Scientific and Technical Information
Springfield, Virginia 22151

FLUTTER STUDIES TO DETERMINE NACELLE AERODYNAMIC EFFECTS ON A FAN-JET TRANSPORT MODEL FOR TWO MOUNT SYSTEMS AND TWO WIND TUNNELS

By Moses G. Farmer
Langley Research Center

SUMMARY

Low-speed flutter studies of a dynamically and elastically scaled model of a large multijet transport airplane have been conducted primarily to determine the nacelle aerodynamic effects of high-bypass-ratio fan-jet engines. Data were obtained on a vertical rod mount in two wind tunnels and on a two-cable mount in one of the tunnels. The flutter response of the model was found to be dependent on nacelle aerodynamics, engine-pylon stiffness, mount-system—wind-tunnel configuration, and mass ratio.

INTRODUCTION

The effects on wing flutter of pylon-mounted masses such as engines and fuel tanks have long been recognized (refs. 1 to 8). Parameters known to be important include both spanwise and chordwise locations as well as mass, inertia, and stiffness properties. The effects of store aerodynamics become important for large stores such as fan-jet engines which have high bypass ratios and are characterized by large-diameter shrouded fans.

This report presents the results of a low-subsonic-speed wind-tunnel investigation, the primary purpose of which was to study the effects of the engine aerodynamic forces on the flutter characteristics of a large multijet transport airplane. Two engine configurations were studied. One consisted of flow-through engine nacelles which were designed to approximately simulate the geometry, inertia, and aerodynamic mass-flow characteristics of the prototype transport engines. The fans of the prototype engines were not simulated. The other configuration consisted of small streamlined bodies (pencil nacelles) attached to the engine pylons in a manner to simulate the engine mass properties while introducing as little aerodynamic input as possible.

Secondary objectives of the investigation were to study the effects on flutter of engine-pylon stiffness, damping, and mass ratio. In addition, the model provided the opportunity for obtaining comparative wind-tunnel-flow information, since the airplane

manufacturer had previously conducted an investigation with this model at the University of Washington Aeronautical Laboratory (UWAL) tunnel. Parts of the previous program were repeated in the Langley transonic dynamics tunnel (TDT) to evaluate the effects of wind-tunnel-flow characteristics. Two different methods of mounting the model were used in the TDT to determine mount-system effects: a vertical rod mount, as was used in the UWAL tunnel, and a two-cable mount.

The effects of Mach number are generally recognized as being important for wings of the type studied in this investigation. However, flutter-prevention programs for new airplanes commonly employ models scaled for low Mach number testing to permit rapid studies of a large number of parameters. Thus, the present study is limited to this commonly used subsonic-flutter-model technique. A brief study of the influence of Mach number on nacelle aerodynamic effects is presented in reference 9.

SYMBOLS

b	half-length of wing mean chord, measured parallel to fuselage center line, 19.14 centimeters
EI	bending stiffness, newton-meters^2
f_C	natural frequency of model structural mode C (values given in table II), hertz
f_f	flutter frequency, hertz
f_l	natural frequency of outboard-engine lateral mode, hertz
GJ	torsional stiffness, newton-meters^2
g	damping coefficient of nacelle modes
M	Mach number
T_{rc}	rear-cable tension, newtons
V	free-stream velocity, meters/second
$\frac{V}{b(2\pi f_C)\sqrt{\mu}}$	flutter-speed index

x	chordwise distance measured from 10.52 centimeters forward of model nose, centimeters
y	spanwise distance measured from fuselage center line, centimeters
ρ	free-stream density, kilograms/meter^3
μ	nondimensional mass-ratio parameter (see p. 7)

Abbreviations:

TDT	Langley transonic dynamics tunnel
UWAL	University of Washington Aeronautical Laboratory

TEST APPARATUS

Wind Tunnels

University of Washington Aeronautical Laboratory (UWAL) tunnel.- The UWAL tunnel is a double-return, closed-circuit tunnel with a solid-wall test section that is 2.44 meters high, 3.66 meters wide, and 3.05 meters long with cropped corners. Tests are conducted in air at atmospheric pressure and subsonic Mach numbers. Reference 10 contains more detailed information.

Langley transonic dynamics tunnel (TDT).- The Langley transonic dynamics tunnel has a 4.88-meter-square test section with cropped corners and is a return-flow, variable-pressure, slotted-wall tunnel. It is capable of operation at stagnation pressures from about 1.3 percent of atmospheric to slightly above atmospheric and at Mach numbers up to 1.2. Mach number and dynamic pressure can be varied independently with either air or Freon-12 used as a test medium. In the present investigation the primary test medium was air although Freon-12 was used in a portion of the investigation to evaluate mass-ratio effects. Freon-12 is almost four times as dense as air at a given pressure and temperature.

Comparison of test sections.- Figure 1 is a scaled drawing which illustrates the relative size of the model and the two wind-tunnel test sections. The cross-sectional areas of the TDT and the UWAL tunnel are 23.08 and 8.51 m^2, respectively. The maximum model cross-sectional area was about 0.10 m^2.

Mount Systems

Vertical rod mount.- Figure 2 is a schematic drawing of the vertical-rod-mount system. A vertical circular rod spanned the tunnel, with the upper and lower portions passing through restraint tubes. Guy wires attached between the restraint tubes and the tunnel walls restricted transverse motions of the rod. A "monkey" which was free to yaw about and to translate vertically along the rod was attached to the model fuselage spar by a pivot which permitted the model to pitch. Thus, the model was free to translate vertically, to pitch, and to yaw. The rod provided elastic restraint in horizontal translation and roll. The extent of the vertical translation was limited to about 70 cm by the restraint tubing which enclosed the rod. To cushion the impact from sudden model vertical excursions, the tubing was attached to shock absorbers at the test-section floor and ceiling.

Two flexible control cables were routed through a system of pulleys and into the tunnel observation chamber where they were used to manually damp out vertical translations of the model. The model was equipped with a remote-control elevator on the right stabilizer which was used to adjust trim and keep lift equal to 80 percent of the model weight as the tunnel speed was changed.

To obtain full-scale airplane Froude numbers and lift coefficients, 20 percent of the model weight was supported by a flexible cable connected to a piston-cylinder mechanism mounted on top of the test section. Air pressure in the cylinder was regulated so that a constant vertical force was applied through the cable.

Figure 3 is a photograph of the model mounted on the vertical rod mount in the TDT. The model is shown temporarily supported at the tunnel center line by a clamp on the rod.

Two-cable mount.- Figure 4 is a schematic drawing of the two-cable-mount mechanism. The model was suspended on two loops of 0.317-cm-diameter steel cable, each of which passed through two pulleys mounted in the fuselage. The forward loop was in a vertical plane with its ends attached to brackets at the floor and ceiling of the test section. The aft cable passed through external pulleys which could be traversed along vertical tracks by remote control. The model was trimmed in roll by traversing these external pulleys in opposite directions. A spring was installed in series with the aft cable to maintain a relatively constant aft-cable tension as model drag loads changed. This mount system restrained fore-and-aft translation and provided a soft spring support in all other degrees of freedom. The right elevator was used to trim the model. Three "snubber" cables were attached to the model fuselage near the center of gravity. These cables were normally slack, but they could be tightened by a pneumatic piston to restrain the model near the tunnel center line if an instability developed.

Figure 5 is a photograph of the model installed on the two-cable-mount system in TDT. The snubber cables are tightened to support the model at the tunnel center line.

Instrumentation

Accelerometers were mounted in the wings, fuselage, and nacelles of the model to sense elastic and rigid-body motions. Strain gages were mounted on the empennage spars to sense static and dynamic loads. Data signals were carried by an umbilical cord shown in figures 3 and 5. The signals were recorded on a tape recorder and were visually monitored on a strip chart.

MODEL

Scaling

The model employed in this investigation was designed to simulate the dynamic and elastic properties of a subsonic transport airplane according to procedures outlined in reference 11. The length scale factor was 0.046. The mass, stiffness, and velocity scale factors selected were such that the reduced frequency and mass ratio of the airplane at a critical altitude were simulated when the model flew at subsonic velocities in air at sea level. For tests conducted on the vertical rod mount, the Froude number was simulated by artificially supporting 20 percent of the model weight. Because the Mach number parameter was not simulated, compressibility effects were not studied. Work such as that described in references 4 to 9, however, has indicated that compressibility effects are very important.

Construction and Stiffness Properties

Wings, fuselage, and empennage.- The wings and fuselage of the model were designed to simulate the mass and stiffness properties of the airplane. A single aluminum spar provided the required bending- and torsional-stiffness distributions for each major structural component. The wing spars were attached to the fuselage spar by a carry-through structure which simulated airplane stiffnesses.

The external contours of the wings and fuselage were obtained with pods which were attached to the spars and separated from each other by foam rubber. The wing pods consisted of balsa frameworks covered with fiber glass. The fuselage pods were primarily wooden shells, stiffened by interior ribs, and covered with fiber glass or tissue paper.

The model empennage was constructed of wood and tissue paper. Mass properties and geometry, but not stiffness, were simulated.

Metal weights were mounted on the spars and in the pods to obtain a mass distribution which simulated the structure, payload, and fuel of the airplane.

Calculated stiffness distributions for the fuselage are shown in figure 6. Similar data for the wings are shown in figure 7 together with details of the wing planform. For

each structure the elastic axis was approximately at the center of the spar. Bending and torsional stiffnesses were calculated for cross sections perpendicular to the elastic axis.

Nacelles and pylons.- Sketches of the inboard and outboard nacelle installations and of a pencil nacelle are shown in figure 8. Figure 9 is a photograph of the engine nacelles.

Each engine nacelle consisted of an aluminum shell with the aft portion covered by thin balsa. Each cowl was machined from balsa, bonded to an aluminum ring at the aft end, and attached to the nacelle by four aluminum struts. The cowls and nacelles were designed to approximately simulate the aerodynamic mass flow through the engine fans but not the internal engine flow. Ballast was added inside the nacelles to simulate mass and inertia characteristics of the airplane engines.

The pencil nacelles were constructed primarily of lead and were designed to simulate the inertia and center-of-gravity characteristics of the engine nacelles.

The engine pylons and pylon mounts were constructed of aluminum. The mounts were bolted rigidly to the wing spar. The side bending stiffness of each pylon was determined by the cross section of the pylon between the mount and the engine. The effects of varying outboard-engine-pylon side bending stiffness were studied by changing pylons. Vertical bending stiffnesses were held constant.

Mass Properties

The mass distribution of the model wing is given in table I together with the masses, spanwise center-of-gravity locations, and moments of inertia for the two kinds of nacelles. (Longitudinal and vertical nacelle center-of-gravity locations are shown in fig. 8.) Engine and pencil nacelles had the same total mass and center-of-gravity positions. The moments of inertia in pitch or yaw were about 10 percent less for a pencil nacelle than for an engine nacelle. The roll inertia of an engine nacelle could not be equaled with a pencil nacelle; however, this fact is believed to be unimportant since flutter primarily involved vertical and lateral motions of the nacelles.

The fuselage mass distributions for the two mount systems are shown in figure 10; the total mass of each fuselage section has been distributed over its length.

For both mount systems, stability considerations were important in positioning the model center of gravity (see figs. 2 and 4). On the vertical rod mount the total model mass was 45.73 kg with the center of gravity at $x = 153.27$ cm. On the two-cable mount the total mass was 45.76 kg with the center of gravity at $x = 157.62$ cm. The pitch and yaw moments of inertia of the model about its center of gravity were almost 5 percent greater on the rod mount than on the two-cable mount.

Frequencies and Mode Shapes

Measured model natural frequencies which were significant for the present investigation are presented in table II. The rigid-body-mode frequencies were different for each mount-system—wind-tunnel combination. The difference in values for the two rod-mount installations was due to the difference in rod lengths.

Flutter data obtained in this investigation involved asymmetric structural modes A, B, and C. The node lines for these modes are shown in figure 11. The natural frequencies and node lines for these nodes were all obtained with the same outboard-engine pylons, for which $f_\ell = 11.29$ hertz. Data obtained by the airplane manufacturer for other vales of f_ℓ have indicated that the characteristics of these three modes are not affected significantly by changes in pylon frequency. While each of these modes involved some vertical and lateral engine motion, the outboard-engine lateral motion of mode B was especially pronounced (see arrows in fig. 11(b)). All three modes involved considerable bending and torsion of the fuselage.

The nacelle-mode frequencies were measured with the pylon mounts attached to a rigid plate.

Nacelle Damping

Two separate methods were used to increase damping of engine-nacelle motions and study the effects of nacelle damping on flutter. In both methods the nominal value of damping coefficient g for both vertical and lateral motion was increased from 0.01 to 0.05.

Viscous damping was added by mounting in each nacelle a capsule which contained oil and a free metal weight. Because of its inertia, the weight tended to remain at rest as the nacelle moved, and damping was induced by the relative motion between the oil and weight.

Friction damping was added by taping several layers of thin balsa strips to the engine pylons.

RESULTS AND DISCUSSION

The data obtained in this investigation are presented in table III and shown in figures 12 to 15.

Values of the mass-ratio parameter μ have been calculated for the wing between $y = 17.06$ cm and $y = 137.17$ cm (see fig. 7). The mass-ratio parameter is defined as the ratio of the mass of the wing excluding nacelles, pylons, and pylon mounts (10.28 kg) to the mass of a volume of the test medium contained in the conical frustums generated by

revolving each wing chord about its midpoint (0.1597 m^3). The mass ratio is shown in the present investigation to affect significantly the model flutter characteristics. Therefore, data presented to show the effects of other parameter variations are at a nearly constant value of mass ratio (54.5 to 57).

In the flutter-speed index $\frac{V}{b(2\pi f_C)\sqrt{\mu}}$, the half-length of the wing mean chord b is 19.14 cm. The values of reference frequency f_C in table II were measured with the same outboard-engine pylons on the three mount-system—wind-tunnel configurations. It has been assumed that the three different values f_C represent the differences in effective model stiffness for all values of outboard-engine pylon frequency.

To determine the accuracy of data, several flutter-test runs were repeated in the TDT and indicated that flutter velocities repeated within an accuracy of 4 percent. The flutter frequencies f_f were measured from oscillograph records within an accuracy of about 5 percent.

For each data point, movie films and oscillograph records were used to determine the structural modes which coupled to form the flutter mode.

Effects of Outboard-Engine Lateral Frequency and Nacelle Aerodynamics

Results from the three mount-system—wind-tunnel configurations are shown in figure 12 and agree as to the primary effects of outboard-engine lateral frequency f_l and nacelle aerodynamic forces. In general, the greatest effects of tuning the outboard pylons occurred when the ratio of the outboard-engine lateral frequency to the reference torsion frequency f_l/f_C was in the region between 1.1 and 1.2, where a change of flutter mode occurred and the highest values of flutter-speed index were obtained for the engine nacelles. The critical value of f_l/f_C varied slightly for the three test configurations and was lower for the pencil nacelles.

For values of f_l/f_C greater than 1.2, the importance of nacelle aerodynamics is shown by an increase of about 20 percent in flutter-speed index for the pencil nacelles over the engine nacelles. Flutter occurred as a result of coupling between structural modes A and C. Slightly higher flutter frequencies were obtained with the pencil nacelles than with the engine nacelles.

For values of f_l/f_C less than 1.1, flutter with the engine nacelles resulted from coupling between structural modes B and C. Structural mode B contributed a large amount of outboard-engine side bending motion to the flutter mode. This flutter mode was not found with the pencil nacelles within the limits of the test, the indication being that nacelle aerodynamic forces were also important for this mode.

Most of the engine-nacelle data presented herein were obtained with viscous damping in the nacelles to provide a damping coefficient g of about 0.05 in the lateral

and vertical nacelle modes. However, some data points were obtained with friction damping ($g \approx 0.05$) and some without damping ($g \approx 0.01$). (For example, see figs. 12(a) and 12(b).) These data indicate that model flutter characteristics were not sensitive to either type or quantity of nacelle damping for the test values of g.

One data point plotted in figure 12(c) was obtained with the cowls removed from the engine nacelles and ballast added in the nacelles equal to the weight of the cowls. The value of flutter-speed index for this configuration was between values obtained for the engine nacelles with cowls and the pencil nacelles.

Comparison of Results for the Two Mount Systems

In figure 13 the ratios of flutter frequency and flutter-speed index for points obtained in the TDT on the two mount systems are plotted as functions of outboard-engine lateral frequency. When repeat runs were available, the lowest value of flutter-speed index was used. The scatter in the flutter-frequency ratios is within the accuracy of the data. The flutter frequencies are shown to be lower on the two-cable mount, as would be expected from the structural-mode natural frequencies (table II).

For values of outboard-engine lateral frequency outside the region where the flutter mode changes, values of flutter-speed index on the two-cable mount are no more than 7 percent greater than values on the vertical rod mount. In the region near 11 hertz, however, differences are as large as 22 percent. The difference in flutter response for the two mount systems may well be due to the difference in fuselage mass distributions shown in figure 10. The 20-percent difference in Froude number may have been a contributing factor.

The effects of varying mount stiffness were studied on the two-cable mount by obtaining a few points at one-half and twice the nominal value of rear-cable tension T_{rc}, which was 890 N. Mount stiffness was approximately proportional to rear-cable tension. Within the accuracy of the data, these stiffness variations did not affect the flutter response of the model.

Comparison of Results for the Two Wind Tunnels

In figure 14 the ratios of flutter frequency and flutter-speed index for points obtained in the two wind tunnels on the vertical rod mount are plotted as functions of outboard-engine lateral frequency. The flutter frequencies are shown to be higher in the TDT, as would be expected from the structural-mode natural frequencies (table II). Flutter-speed-index values obtained in the TDT are consistently greater than in the UWAL tunnel, by as much as about 9 percent for the engine nacelles and 15 percent for the pencil nacelles. The following factors may have contributed to the difference in results for the two tunnels.

Tunnel-wall effects may have distorted the flow about the model. According to reference 12, blockage corrections are less than one-half of 1 percent for both tunnels, and since for both tunnels the model span is less than 80 percent of test-section width (fig. 1), spanwise lift distortions are insignificant. Approximate steady-state correction factors have been calculated for distortions of wing lift-curve slope by using the methods of reference 12 for UWAL data and the method of reference 13 for TDT data. With flutter speed assumed to be inversely proportional to lift-curve slope, these corrections indicate that wall effects reduce flutter speed in the UWAL tunnel by about 4 percent and increase flutter speed in the TDT by about 1 percent to account for about a 5-percent difference. To investigate analytically the unsteady wall effects would require a flutter analysis with superimposed wall boundary conditions. Reference 14 discusses procedures which may be used to estimate interference effects on airfoils caused by forced sinusoidal pitch oscillations at low frequencies; however, these procedures are not adequate for the complex, self-excited motions of the present model.

The observed character of the model response to the airflow prior to flutter was different in the two tunnels. In the UWAL tunnel there was considerable random excitation of the model. In the less turbulent TDT, the model exhibited very little response even though attempts were frequently made to excite flutter with the control cables.

Effects of Mass Ratio

Mass-ratio effects have been studied for many years and it has long been recognized that they can be significant (see, for example, refs. 15 and 16). Most of the experimental evidence available concerning mass-ratio effects is limited to relatively simple wings, and there have been very few studies of mass-ratio effects on complex, complete-vehicle flutter of the type considered in this investigation. Therefore, in the present investigation mass-ratio effects were studied on the vertical rod mount in the TDT by using air and Freon-12 at several densities. The resulting data, which are plotted in figure 15, were obtained by using the engine nacelles without damping. Two values of f_l/f_f were used. It is noteworthy that there is good agreement between data in air and Freon-12 even though Mach numbers are different for comparable points in the two gases.

For both values of f_l/f_f, the variation of flutter-speed index with mass ratio μ was significant for values of mass ratio less than about 150. When the mass ratio is less than about 30, where the two curves cross, the greater value of flutter-speed index is obtained with the larger value of f_l/f_f.

The flutter frequencies appear to vary slightly with mass ratio.

CONCLUSIONS

Low-speed flutter studies of a dynamically and elastically scaled model of a large multijet transport airplane have been conducted. Although the effects of Mach number were not studied in this investigation and it is realized that this variable may significantly influence flutter characteristics, the following conclusions from this low-speed investigation are believed to be significant:

(1) Nacelle aerodynamic forces for the simulated high-bypass-ratio fan-jet engines caused about a 20-percent reduction in flutter-speed index.

(2) Model flutter characteristics were greatly dependent on outboard-engine lateral frequency.

(3) Values of flutter-speed index obtained on a two-cable-mount system were no more than 7 percent greater than values obtained on a vertical rod mount except for a region of outboard-engine lateral frequencies where the flutter mode changed and differences in flutter-speed index of as much as 22 percent occurred; the differences in flutter response for the two mount systems may well be due to the significant differences in fuselage mass distributions.

(4) Values of flutter-speed index obtained in the slotted-wall Langley transonic dynamics tunnel were up to 15 percent greater than those obtained in the relatively small, solid-wall University of Washington Aeronautical Laboratory tunnel.

(5) The variation of flutter-speed index with mass ratio was significant at mass ratios less than about 150.

Langley Research Center,
National Aeronautics and Space Administration,
Hampton, Va., August 7, 1970.

REFERENCES

1. Beckley, Lawrence E.; and Johnson, H. Clay, Jr.: An Experimental Investigation of the Flutter of a Tapered Wing With Simulated Engines, Tip Float and Tip Tank. Bur. Aero. Contract No. NOa(s)7493, Aero-Elastic Res. Lab., M.I.T., Nov. 15, 1947.

2. Andropoulos, T. C.; Chee, C. F.; and Targoff, W. P.: The Effects of Engine Locations on the Antisymmetric Flutter Mode. *AF Tech. Rep. No. 6353, Wright Air Develop.* Center, U.S. Air Force, Aug. 1951.

3. Gaukroger, D. R.: Flutter Characteristics of a Wing Carrying a Flexibly Mounted Mass. R. & M. No. 3330, British A.R.C., 1963.

4. Ruhlin, Charles L.; and Boswinkle, Robert W., Jr.: Transonic Flutter Investigation of a Cantilevered, Aspect-Ratio-4, 45° Sweptback, Uptapered Wing With Three Different Pylon-Mounted External-Store Configurations. NACA RM L57E23, 1957.

5. Yates, E. Carson, Jr.: Theoretical Investigation of the Subsonic and Supersonic Flutter Characteristics of a Swept Wing Employing a Tuned Sting-Mass Flutter Suppressor. NASA TN D-542, 1960.

6. Levey, G. M.; Tuovila, W. J.; and Rainey, A. G.: An Experimental Study of the Effect of Rearward Mounted Heavy Nacelles on the Flutter Characteristics of Low-Aspect-Ratio Wings at Transonic and Supersonic Speeds. NASA TM X-555, 1961.

7. Young, Lou S.; and Ruhlin, Charles L.: Effect of Store Pitch Flexibility on Flutter Characteristics of a Wing-Store Configuration at Mach Numbers Near 0.85. NASA TN D-2479, 1964.

8. Bensinger, C. T.: 1/8 Scale FB-111 Flutter Model Test With SRAMs, 600 Gallon Tanks, and B-43, B-61, and B-57 Weapons. FZS-12-6051, (Contract AF33(657)-8260,) Gen. Dyn./Ft. Worth, Oct. 17, 1969.

9. Rainey, A. Gerald: Aeroelastic Considerations for Transports of the Future – Subsonic, Supersonic, and Hypersonic. AIAA Pap. No. 68-215, Feb. 1968.

10. Anon.: Detailed Information on UWAL Wind Tunnel Model Installation, Test Procedures, and Auxiliary Equipment. UWAL Wind Tunnel Brochure, Univ. of Washington, Apr. 1, 1964.

11. Bisplinghoff, Raymond L.; Ashley, Holt; and Halfman, Robert L.: Aeroelasticity. Addison-Wesley Pub. Co., Inc., c.1955.

12. Pope, Alan: Wind-Tunnel Testing. Second ed., John Wiley & Sons, Inc., c.1954.

13. Davis, Don D., Jr.; and Moore, Dewey: Analytical Study of Blockage- and Lift-Interference Corrections for Slotted Tunnels Obtained by the Substitution of an Equivalent Homogeneous Boundary for the Discrete Slots. NACA RM L53E07b, 1953.

14. Garner, H. C.; Moore, A. W.; and Wight, K. C.: The Theory of Interference Effects on Dynamic Measurements in Slotted-Wall Tunnels at Subsonic Speeds and Comparisons With Experiment. R. & M. No. 3500, Brit. A.R.C., 1968.

15. Yates, E. Carson, Jr.: Modified-Strip-Analysis Method for Predicting Wing Flutter at Subsonic to Hypersonic Speeds. J. Aircraft, vol. 3, no. 1, Jan.-Feb. 1966, pp. 25-29.

16. Yates, E. Carson, Jr.: Subsonic and Supersonic Flutter Analysis of a Highly Tapered Swept-Wing Planform, Including Effects of Density Variation and Finite Wing Thickness, and Comparison With Experiments. NASA TN D-4230, 1967.

TABLE I.- WING AND NACELLE MASS PROPERTIES

Component	y, cm (a)	Mass, kg	Roll inertia, kg-cm^2 (b)	Pitch inertia, kg-cm^2 (b c)
Wing section 1	24.13	3.90		
Wing section 2	39.67	2.50		
Wing section 3	54.71	1.18		
Strut and mount	54.92	.39		
Inboard nacelles:				
Engine	54.92	.87	11.26	30.23
Pencil (alternate)	54.92	.87	.58	26.83
Wing section 4	67.69	1.06		
Wing section 5	79.65	.81		
Wing section 6	90.11	.36		
Strut and mount	97.44	.35		
Outboard nacelles:				
Engine	97.44	.87	11.15	30.35
Pencil (alternate)	97.44	.87	.58	26.83
Wing section 7	104.39	.28		
Wing section 8	113.99	.08		
Wing section 9	123.65	.06		
Wing section 10	132.59	.05		

[a]At component center of gravity.

[b]About an axis through component center of gravity.

[c]Also approximate yaw inertia.

TABLE II.- MODEL NATURAL FREQUENCIES

Mode	Rod mount in UWAL tunnel		Rod mount in TDT		Two-cable mount in TDT (a)	
Rigid-body modes						
	Frequency, Hz					
Side translation	2.80		1.52		0.48	
Fore and aft translation	2.80		1.52		High	
Vertical translation	0		0		.38	
Roll	1.39		1.19		.83	
Pitch	0		0		1.35	
Yaw	0		0		1.10	
Model structural modes[b]						
	Frequency, Hz	Damping coefficient	Frequency, Hz	Damping coefficient	Frequency, Hz	Damping coefficient
Asymmetric wing bending, mode A	6.00	0.020	6.10	0.019	5.90	0.023
Asymmetric wing bending, mode B	7.21	.013	7.41	.029	7.15	.020
Asymmetric wing torsion, mode C	[c]8.84	.026	[c]9.05	.027	[c]8.90	.033
Symmetric wing bending	3.9 (nominal)		3.9 (nominal)		3.9 (nominal)	
Symmetric wing torsion	9.0 (nominal)		9.0 (nominal)		9.0 (nominal)	
Nacelle modes						
	Frequency, Hz					
Inboard-nacelle vertical mode	13.91		13.91		13.91	
Inboard-nacelle lateral mode	9.05		9.05		9.05	
Outboard-nacelle vertical mode	18.68		18.68		18.68	
Outboard-nacelle lateral mode	[d]8.47 to 20.34		[d]8.47 to 20.34		[d]8.47 to 20.34	

[a]Rear-cable tension was 890 N.

[b]With engine nacelles, viscous damping, and f_l = 11.29 Hz.

[c]Reference frequency f_C.

[d]Test variable f_l.

TABLE III.- COMPILATION OF TEST RESULTS

(a) UWAL vertical-rod-mount data in air (f_C = 8.84)

ρ, kg/m^3	V, m/s	M	μ	$\frac{V}{b(2\pi f_C)\sqrt{\mu}}$	f_l, Hz	f_l/f_C	f_f, Hz	f_f/f_C
Engine nacelles without damping (g ≈ 0.01)								
1.17	59.62	----	55.00	0.756	8.39	0.949	8.1	0.916
1.17	67.88	----	55.00	.861	9.67	1.094	8.4	.950
1.17	56.14	----	55.00	.712	10.46	1.183	7.2	.814
Engine nacelles with viscous damping (g ≈ 0.05)								
1.17	61.78	----	55.00	0.784	8.47	0.958	8.0	0.905
1.18	70.77	----	54.53	.901	9.84	1.113	8.1	.916
1.17	71.84	----	55.00	.911	10.59	1.198	--	----
1.17	54.62	----	55.00	.693	11.04	1.249	7.2	.814
1.16	53.64	----	55.47	.677	11.29	1.277	7.2	.814
1.17	53.64	----	55.00	.680	11.75	1.329	7.3	.826
1.16	54.31	----	55.47	.686	12.54	1.418	7.2	.814
1.16	52.67	----	55.47	.665	14.03	1.587	7.3	.826
1.17	53.28	----	55.00	.676	20.34	2.301	7.3	.826
Pencil nacelles (g ≈ 0.01)								
1.16	70.41	----	55.47	0.889	8.47	0.958	--	----
1.16	64.13	----	55.47	.810	9.84	1.113	7.5	0.848
1.16	64.13	----	55.47	.810	10.59	1.198	7.5	.848
1.15	63.46	----	55.96	.798	12.54	1.418	7.5	.848
1.16	62.18	----	55.47	.785	14.03	1.587	7.5	.848
1.15	62.91	----	55.96	.791	20.34	2.301	7.5	.848

(b) TDT vertical-rod-mount data in Freon-12 (f_C = 9.05)

ρ, kg/m^3	V, m/s	M	μ	$\frac{V}{b(2\pi f_C)\sqrt{\mu}}$	f_l, Hz	f_l/f_C	f_f, Hz	f_f/f_C
Engine nacelles without damping (g ≈ 0.01)								
0.67	81.38	0.527	96.04	0.763	8.39	0.927	8.2	0.906
1.11	66.78	.432	57.97	.806	8.39	.927	8.2	.906
1.48	59.07	.382	43.48	.823	8.39	.927	8.1	.895
1.91	53.83	.348	33.69	.852	8.39	.927	8.1	.895
2.15	50.84	.329	29.93	.854	8.39	.927	8.1	.895
.68	65.32	.422	94.63	.617	11.75	1.298	7.3	.807
1.13	56.51	.365	56.95	.688	11.75	1.298	7.3	.807
1.51	53.46	.347	42.62	.752	11.75	1.298	7.3	.807
1.92	55.29	.359	33.52	.877	11.75	1.298	7.3	.807
2.15	53.55	.347	29.93	.899	11.75	1.298	7.5	.829

TABLE III.- COMPILATION OF TEST RESULTS – Continued

(c) TDT vertical-rod-mount data in air (f_C = 9.05)

ρ, kg/m^3	V, m/s	M	μ	$\frac{V}{b(2\pi f_C)\sqrt{\mu}}$	f_l, Hz	f_l/f_C	f_f, Hz	f_f/f_C
Engine nacelles without damping (g ≈ 0.01)								
1.19	64.59	0.186	54.08	0.807	8.39	0.927	8.2	0.906
1.15	65.23	.187	55.96	.801	8.39	.927	8.1	.895
.77	77.69	.224	83.57	.781	8.39	.927	8.2	.906
.28	122.59	.354	229.82	.743	8.39	.927	8.3	.917
.12	173.67	.506	536.25	.689	8.39	.927	8.5	.939
1.14	57.61	.165	56.45	.704	11.75	1.298	7.2	.796
.74	65.71	.188	86.96	.647	11.75	1.298	7.3	.807
.28	94.58	.272	229.82	.573	11.75	1.298	7.2	.796
.12	133.87	.386	536.25	.531	11.75	1.298	7.2	.796
1.16	72.54	.209	55.47	.895	9.67	1.068	8.4	.928
1.15	81.41	.234	55.96	1.000	10.46	1.156	8.5	.939
Engine nacelles with viscous damping (g ≈ 0.05)								
1.15	65.62	0.188	55.96	0.806	8.47	0.936	8.2	0.906
1.15	66.11	.189	55.96	.812	8.47	.936	8.2	.906
1.15	69.34	.199	55.96	.852	8.80	.972	8.4	.928
1.13	75.01	.214	56.95	.913	9.84	1.087	8.3	.917
1.14	74.40	.213	56.45	.910	9.84	1.087	8.3	.917
1.13	83.15	.238	56.95	1.012	10.59	1.170	8.4	.928
1.15	61.23	.175	55.96	.752	11.04	1.220	7.3	.807
1.14	62.70	.179	56.45	.767	11.04	1.220	7.2	.796
1.14	62.06	.177	56.45	.759	11.29	1.248	7.4	.818
1.14	59.95	.171	56.45	.733	11.29	1.248	7.4	.818
1.14	60.12	.171	56.45	.735	11.75	1.298	7.4	.818
1.14	58.52	.167	56.45	.716	12.54	1.386	7.2	.796
1.14	58.80	.168	56.45	.719	14.03	1.550	7.3	.807
1.14	58.95	.168	56.45	.721	20.34	2.248	7.3	.807
Engine nacelles with friction damping (g ≈ 0.05)								
1.17	70.71	0.204	55.00	0.876	9.05	1.000	8.0	0.884
1.15	81.02	.233	55.96	.995	10.38	1.147	8.4	.928
1.17	63.15	.182	55.00	.782	11.13	1.230	7.2	.796
Pencil nacelles (g ≈ 0.01)								
1.14	82.94	0.237	56.45	1.014	8.47	0.936	--	----
1.14	83.00	.238	56.45	1.015	9.84	1.087	--	----
1.14	75.86	.217	56.45	.927	10.59	1.170	7.6	0.840
1.14	71.20	.204	56.45	.871	12.54	1.386	7.6	.840
1.14	70.96	.203	56.45	.868	14.03	1.550	7.6	.840
1.14	72.48	.206	56.45	.886	20.34	2.248	7.7	.851

TABLE III.- COMPILATION OF TEST RESULTS – Concluded

(d) TDT two-cable-mount data in air (f_C = 8.90)

ρ, kg/m^3	V, m/s	M	μ	$\frac{V}{b(2\pi f_C)\sqrt{\mu}}$	f_l, Hz	f_l/f_C	f_f, Hz	f_f/f_C	T_{rc}, N
Engine nacelles with viscous damping (g ≈ 0.05)									
1.17	66.17	0.191	55.00	0.834	8.47	0.952	8.1	0.910	890
1.15	66.90	.192	55.96	.836	8.47	.952	8.1	.910	890
1.15	66.90	.192	55.96	.836	8.47	.952	8.1	.910	445
1.15	76.63	.221	55.96	.957	9.84	1.106	8.2	.921	890
1.15	79.83	.230	55.96	.997	10.59	1.190	--	----	890
1.14	84.03	.241	56.45	1.045	10.59	1.190	--	----	890
1.17	67.18	.194	55.00	.846	11.04	1.240	7.3	.820	890
1.16	67.88	.195	55.47	.852	11.29	1.268	7.3	.820	890
1.15	70.16	.202	55.96	.876	11.29	1.268	7.3	.820	890
1.15	71.60	.205	55.96	.894	11.29	1.268	7.1	.798	445
1.17	61.97	.178	55.00	.781	11.75	1.320	7.2	.809	890
1.15	63.61	.182	55.96	.794	11.75	1.320	7.2	.809	890
1.14	64.80	.185	56.45	.806	11.75	1.320	7.1	.798	445
1.15	64.01	.183	55.96	.800	11.75	1.320	7.2	.809	1335
1.17	62.03	.179	55.00	.781	12.54	1.409	7.2	.809	890
1.17	60.84	.176	55.00	.766	14.03	1.576	7.4	.831	890
1.15	59.89	.171	55.96	.748	20.34	2.285	7.2	.809	890
Engine nacelles with cowls removed (g ≈ 0.01)									
1.15	68.15	0.195	55.96	0.851	12.54	1.409	7.4	0.831	890
Pencil nacelles (g ≈ 0.01)									
1.14	75.96	0.217	56.45	0.945	9.84	1.106	7.4	0.831	890
1.14	75.25	.215	56.45	.936	9.84	1.106	7.5	.843	890
1.14	76.47	.219	56.45	.951	10.59	1.190	7.4	.831	890
1.14	72.66	.208	56.45	.904	12.54	1.409	7.5	.843	890

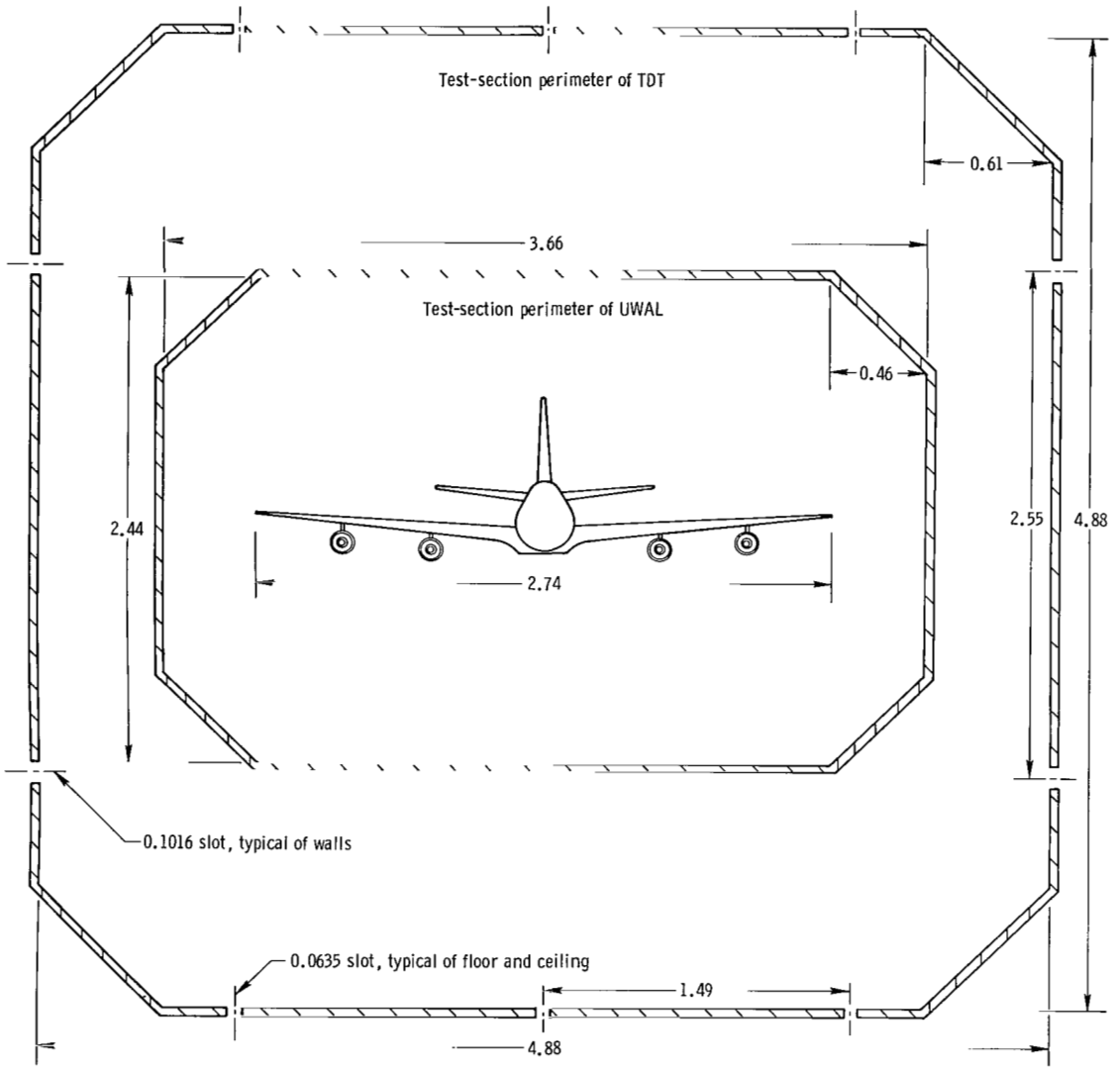

Figure 1.- Cross-sectional view of model in wind-tunnel test sections.
(All dimensions are in meters.)

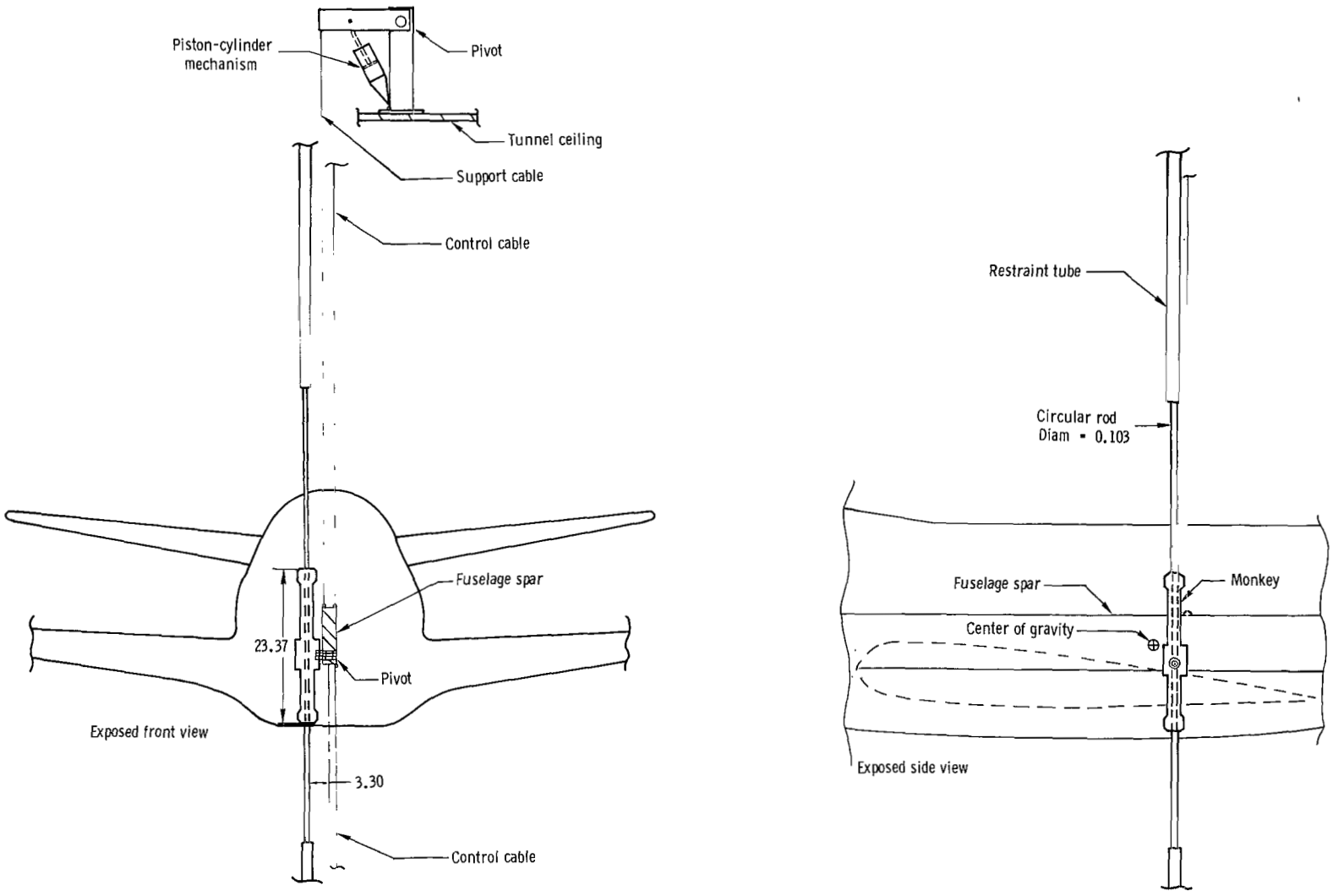

Figure 2.- Schematic drawing of the vertical-rod-mount installation. (All dimensions are in cm.)

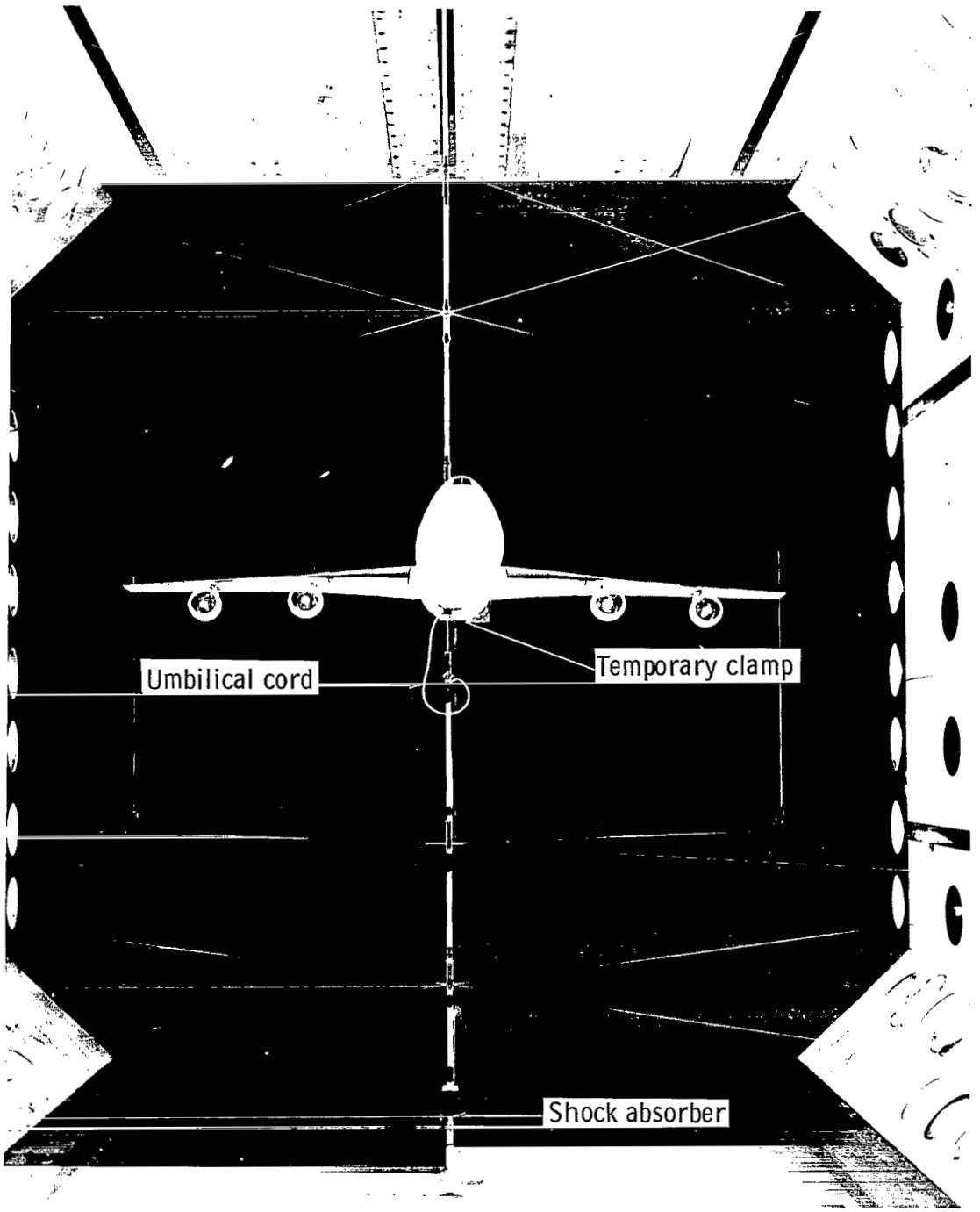

L-67-7213.1

Figure 3.- Model installed in the TDT on the vertical rod mount.

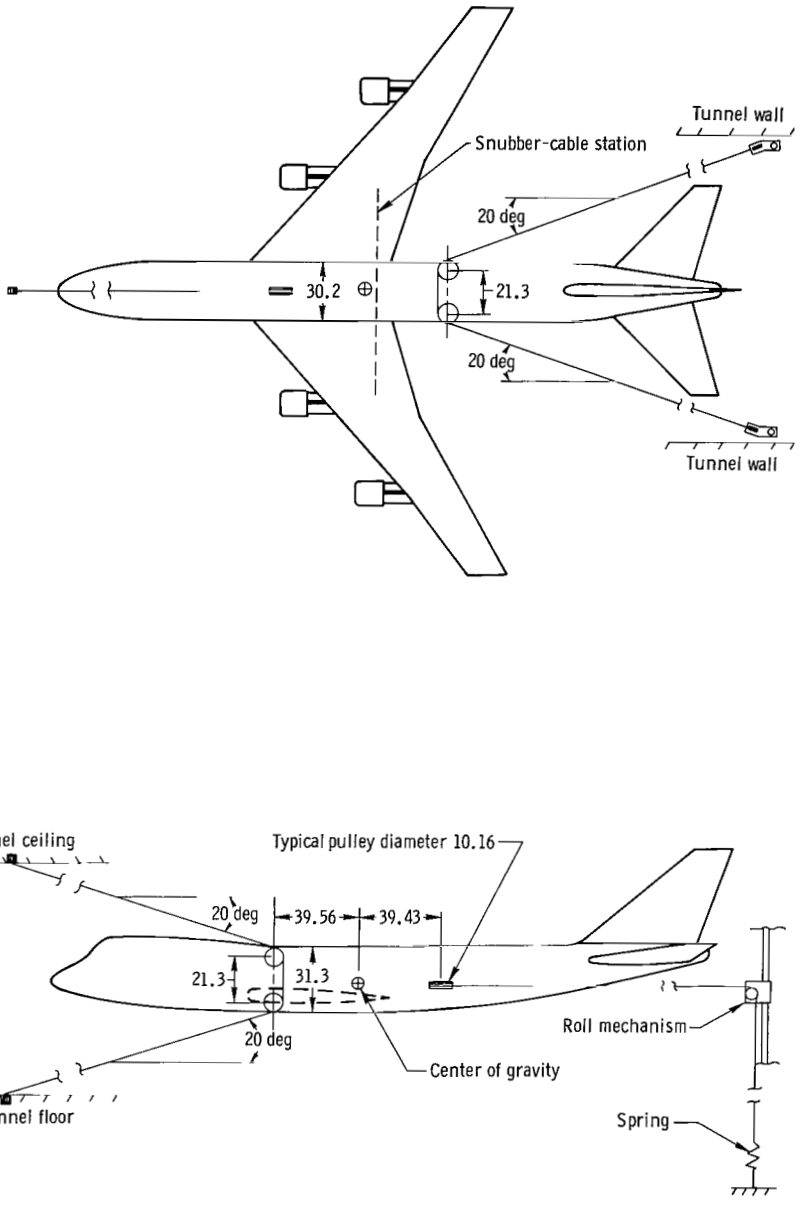

Figure 4.- Schematic drawing of the two-cable-mount installation. (All dimensions are in cm.)

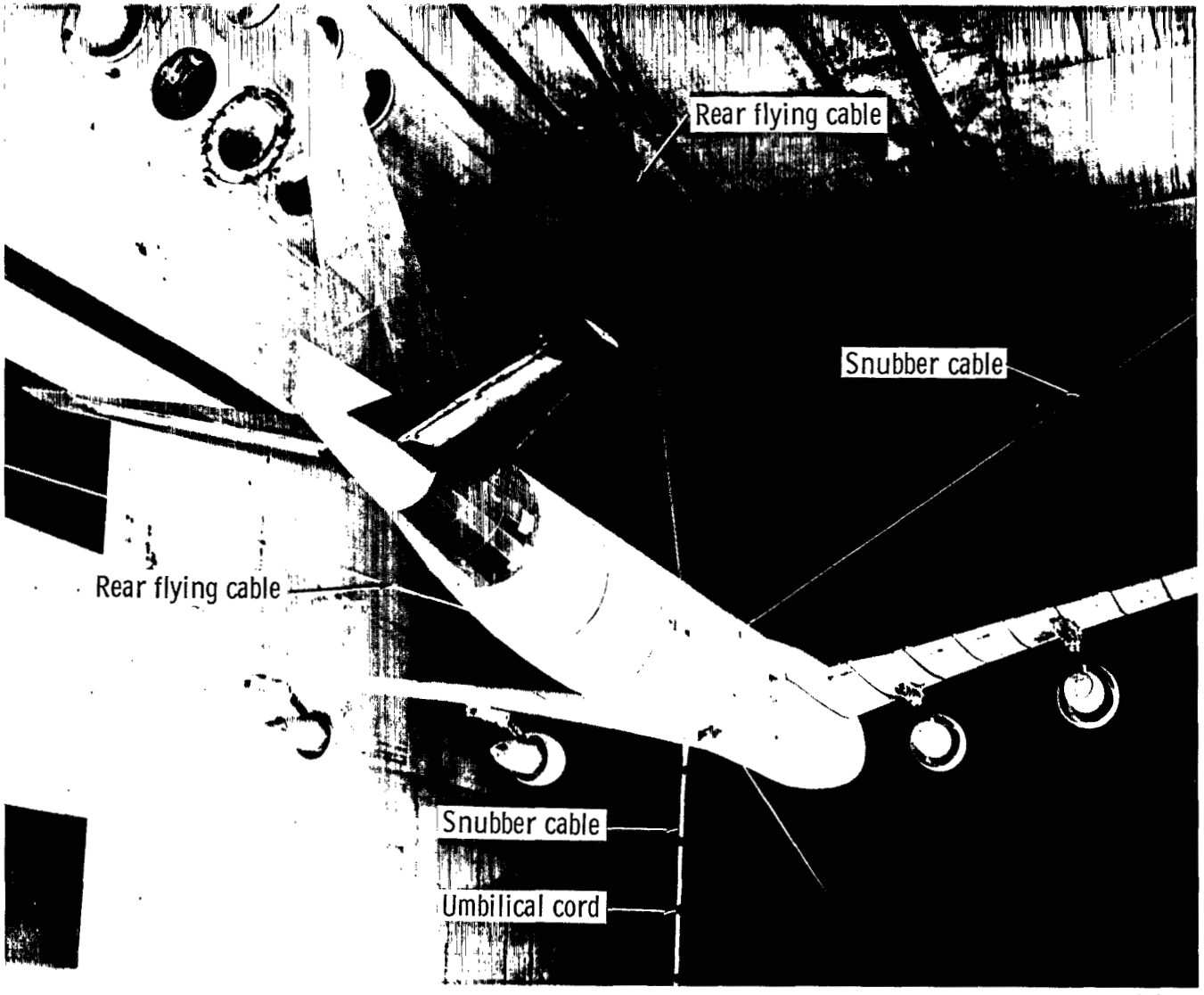

L-67-7608.1

Figure 5.- Model installed in the TDT on the two-cable mount.

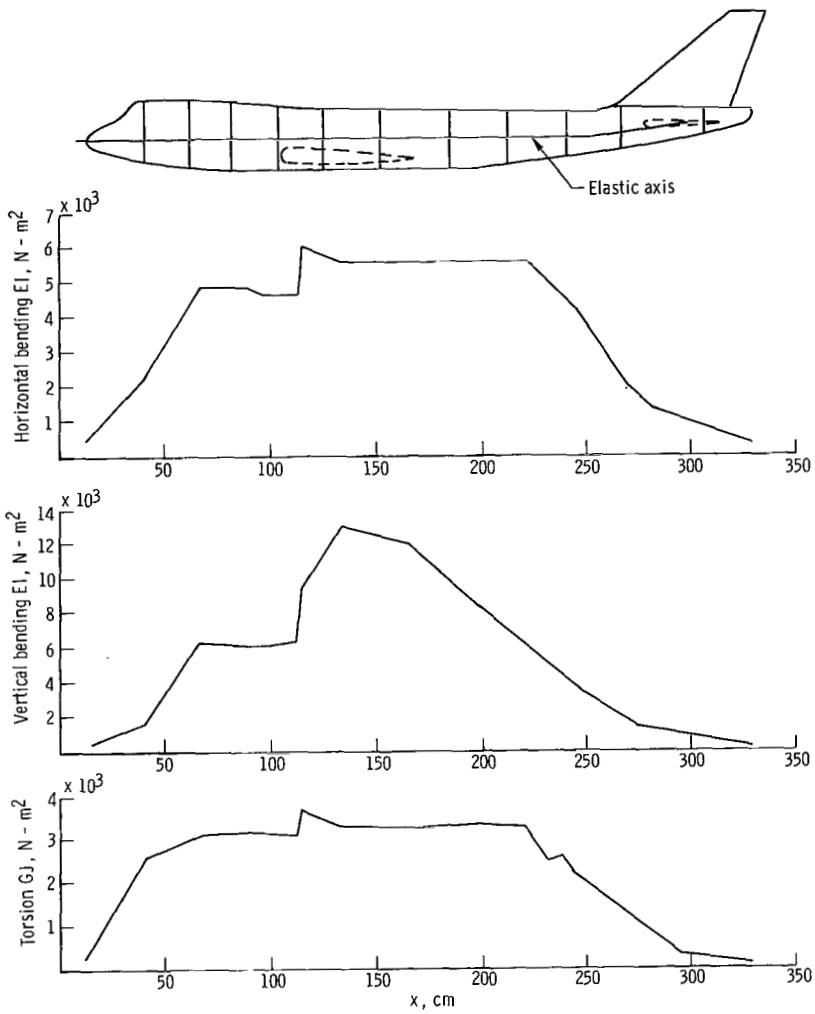

Figure 6.- Fuselage stiffness characteristics.

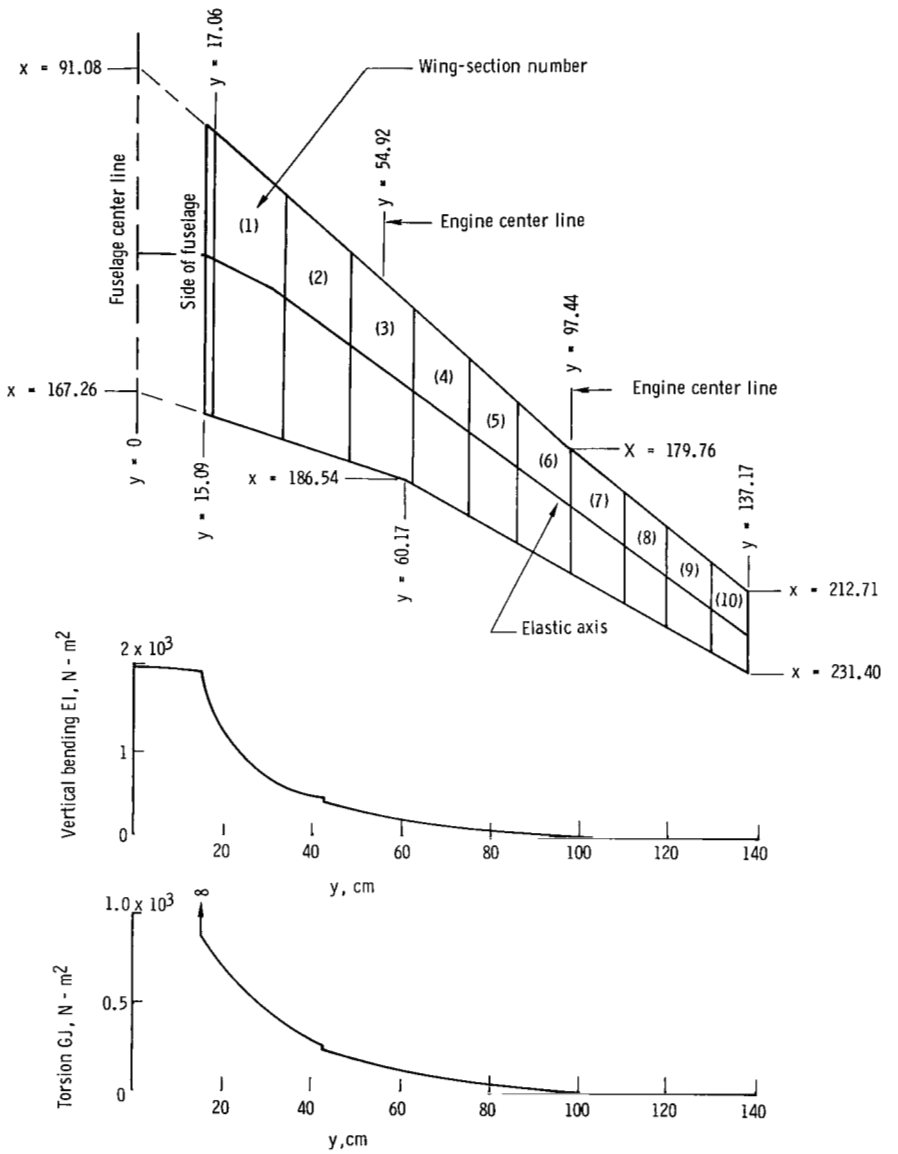

Figure 7.- Wing planform and stiffness characteristics.
(All dimensions are in cm.)

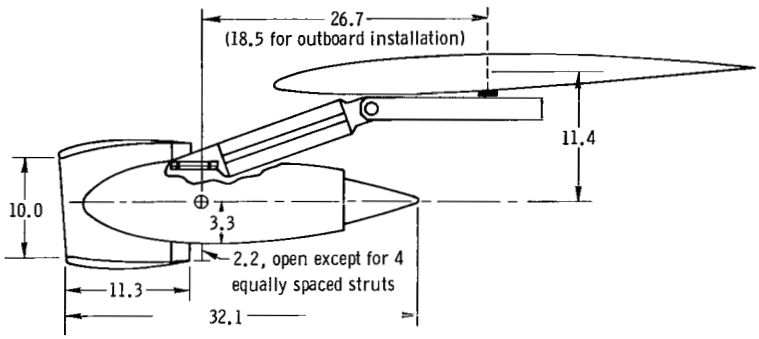

(a) Inboard engine-nacelle installation.

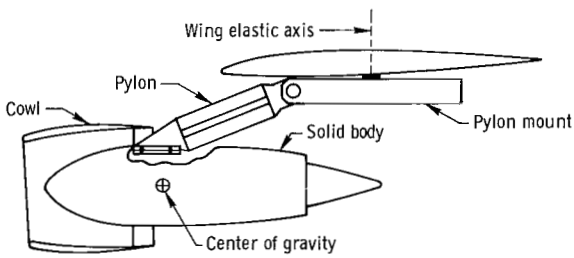

(b) Outboard engine-nacelle installation.

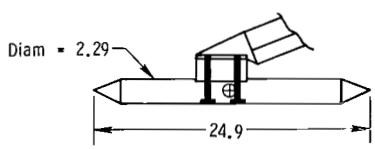

(c) Pencil-nacelle installation.

Figure 8.- Sketches of nacelles and struts. (All dimensions are in cm.)

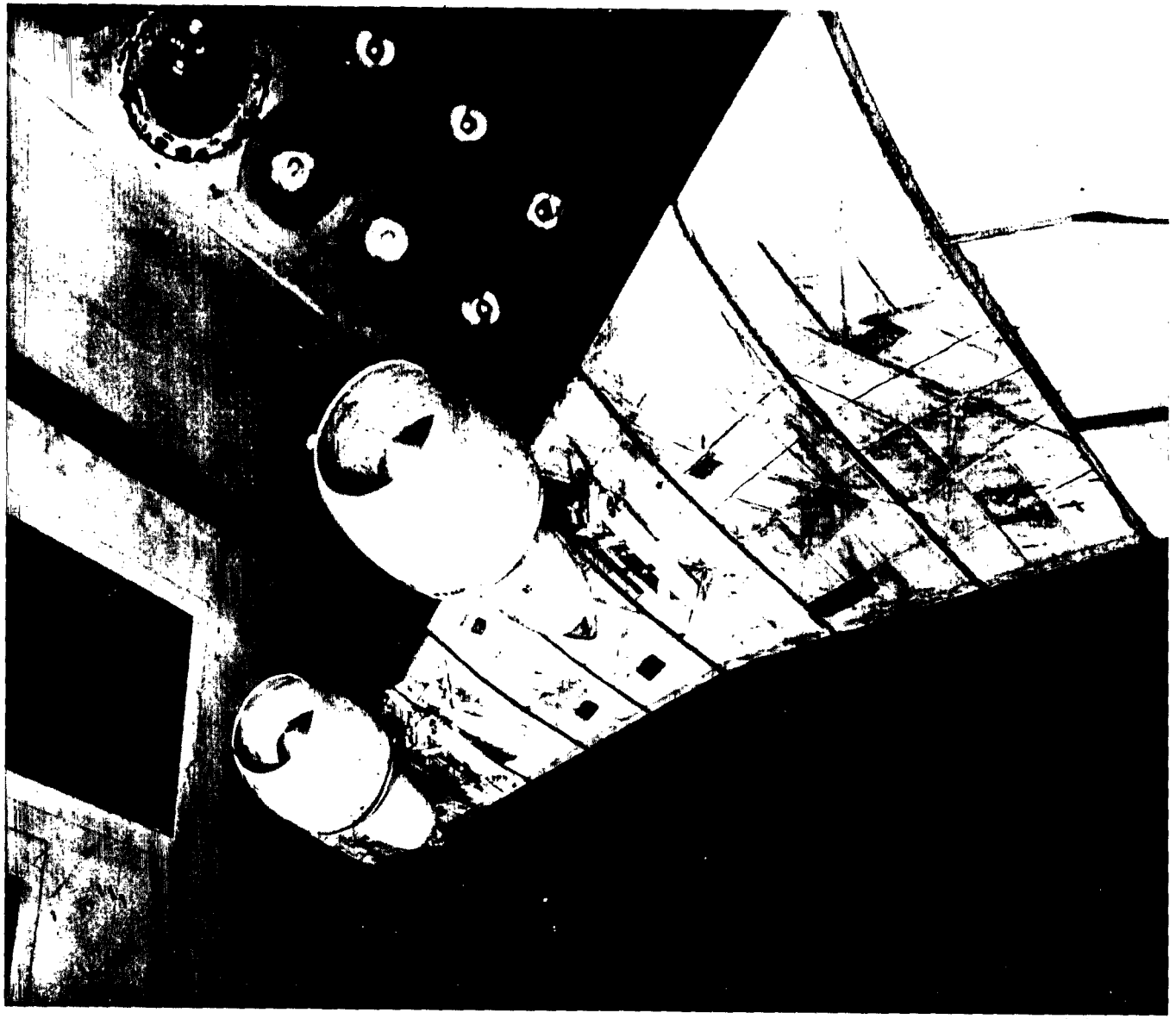

L-67-7215

Figure 9.- Engine nacelles installed on the model.

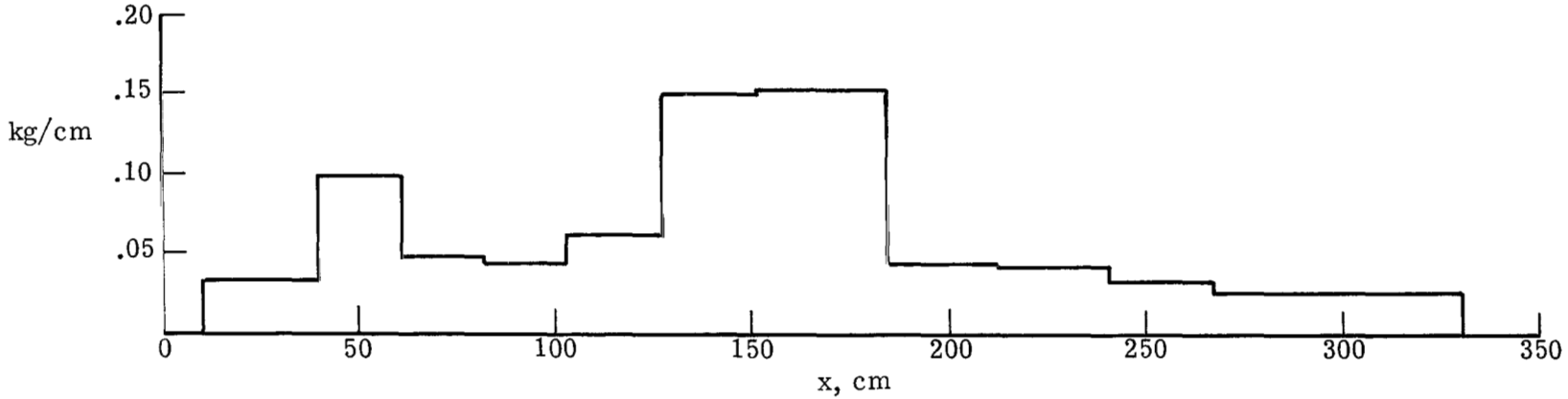

(a) Vertical rod mount.

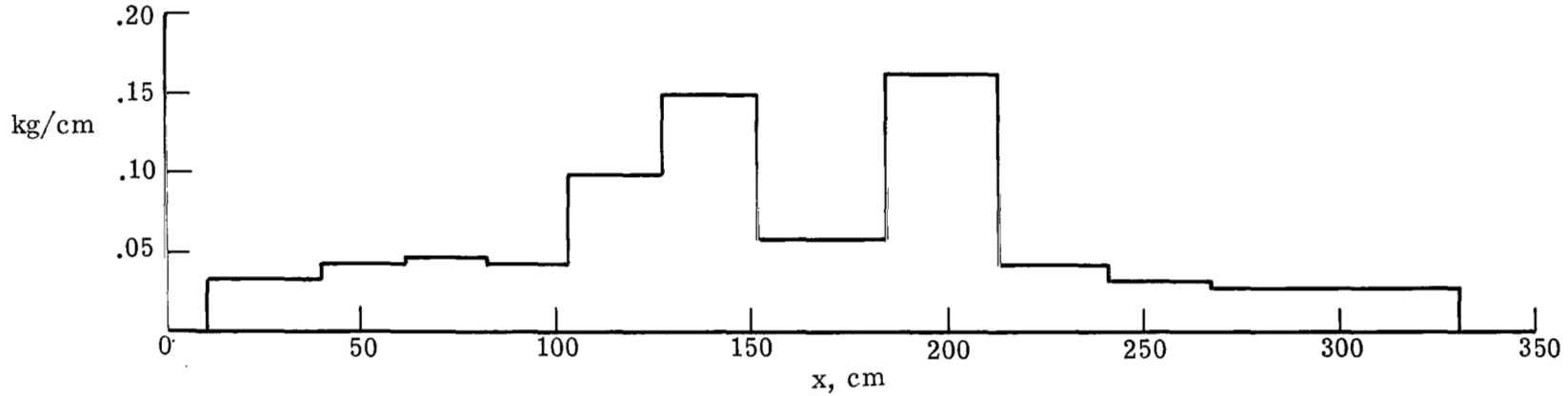

(b) Two-cable mount.

Figure 10.- Fuselage mass distributions. (The differences in the two mass distributions are due to the different masses of the two mount systems.)

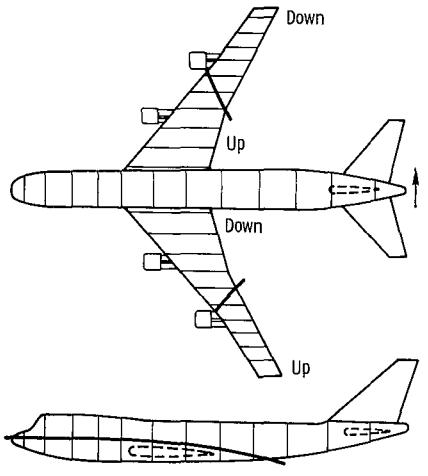

(a) Mode A (asymmetric wing bending).

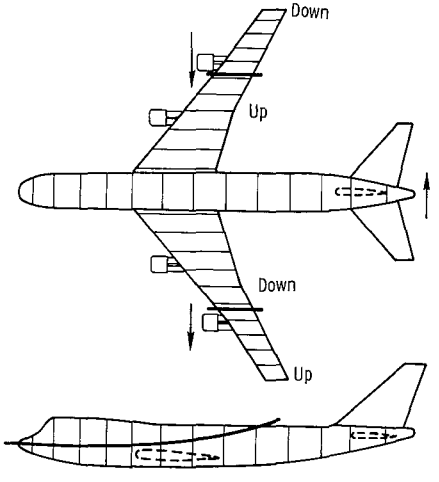

(b) Mode B (asymmetric wing bending).

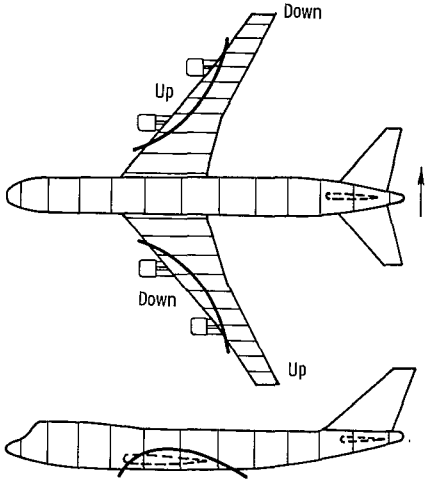

(c) Mode C (asymmetric wing torsion).

Figure 11.- Node lines of important structural modes.

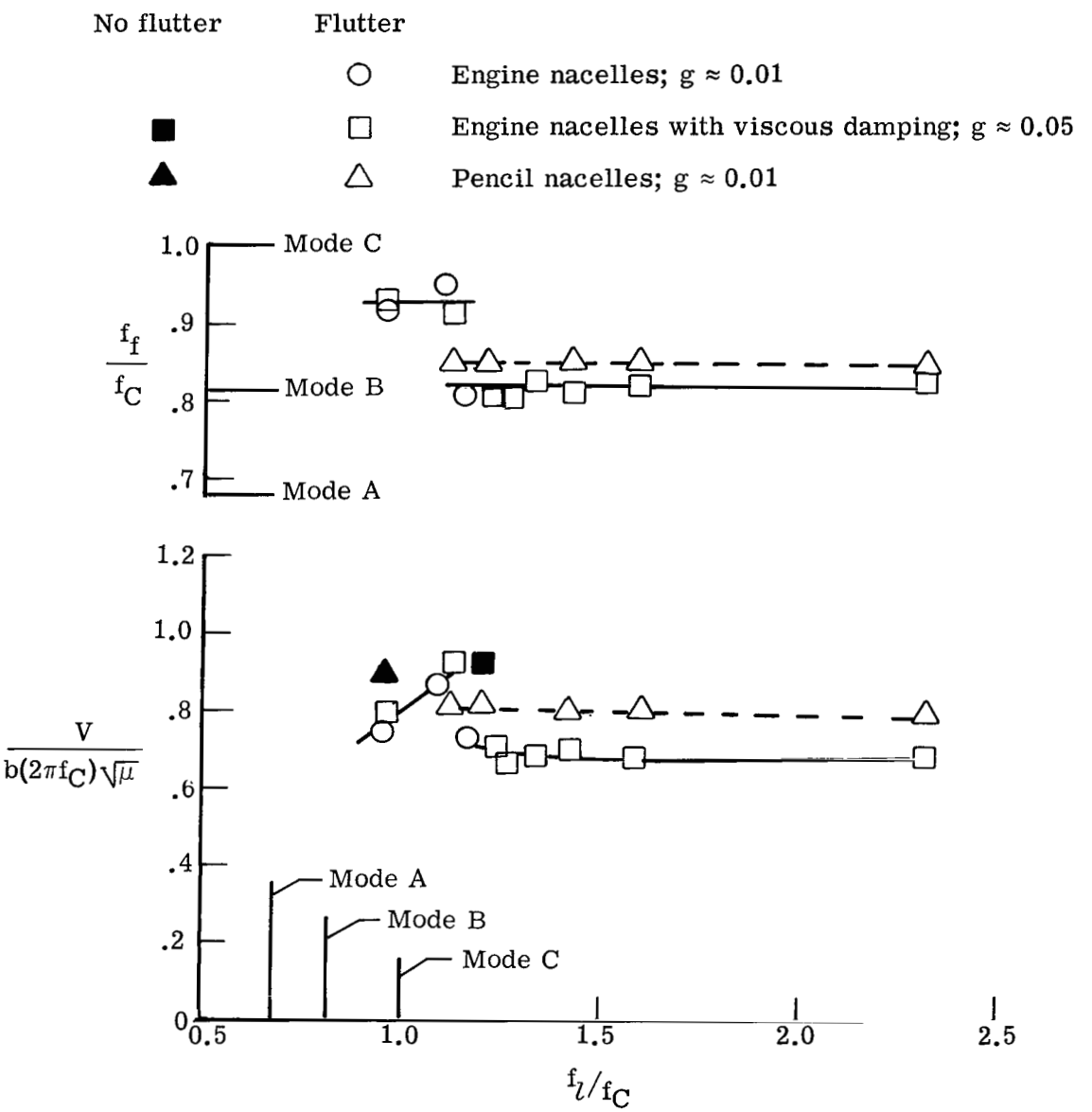

(a) Results obtained on the vertical rod mount in the UWAL tunnel.

Figure 12.- Effects of f_l and nacelle aerodynamics.

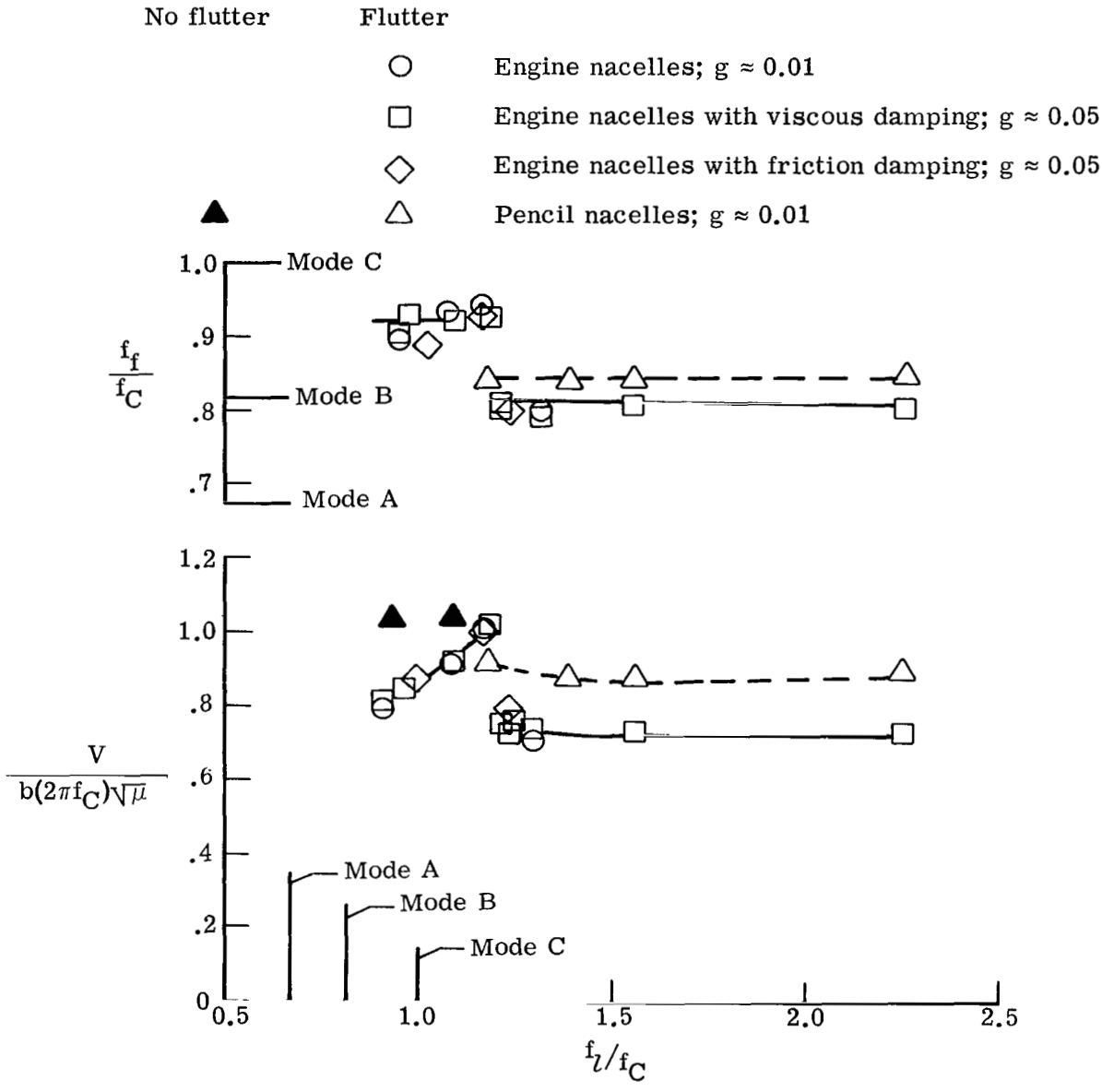

(b) Results obtained on the vertical rod mount in the TDT.

Figure 12.- Continued.

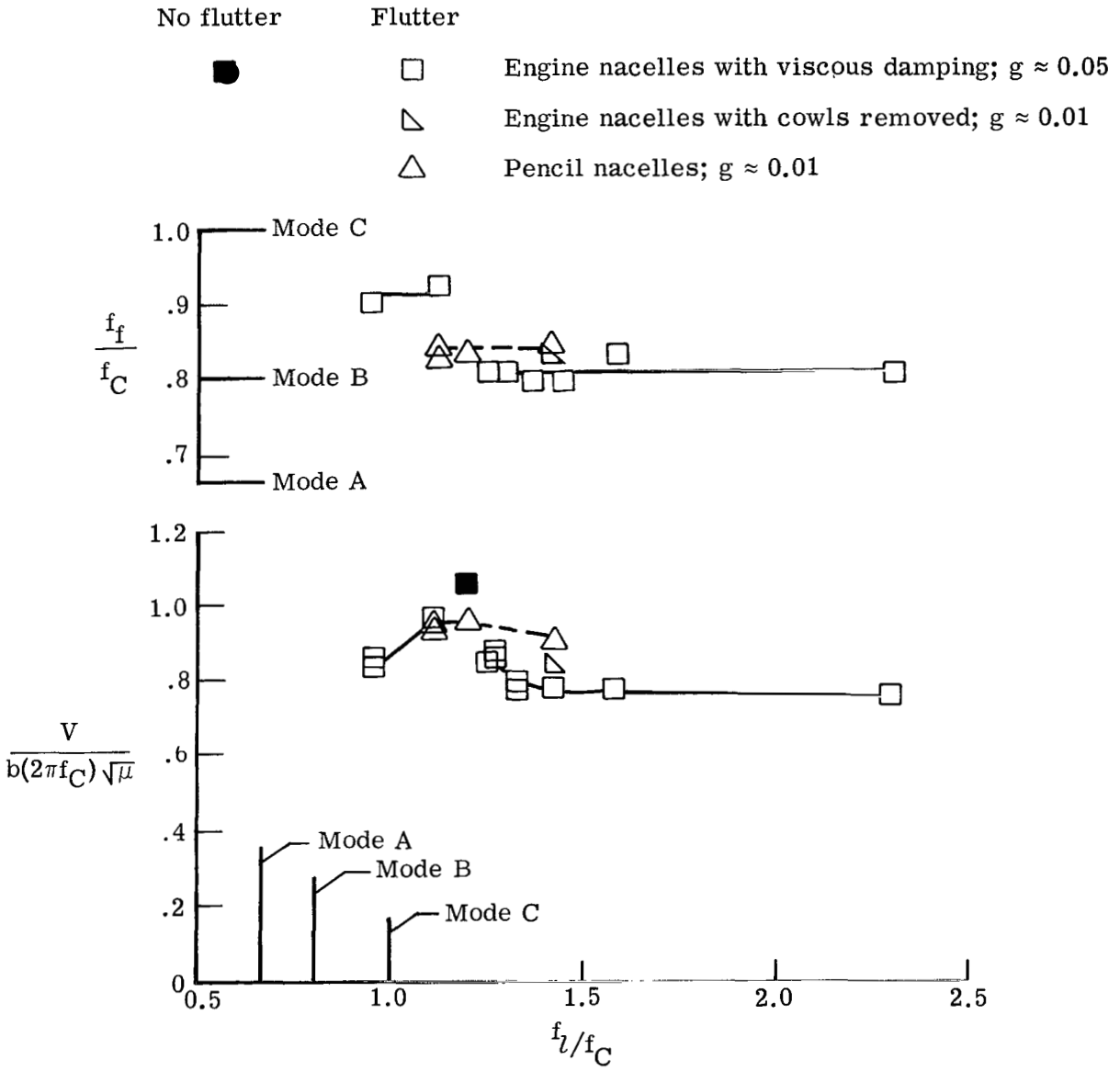

(c) Results obtained on the two-cable mount in the TDT; T_{rc} = 890 N.

Figure 12.- Concluded.

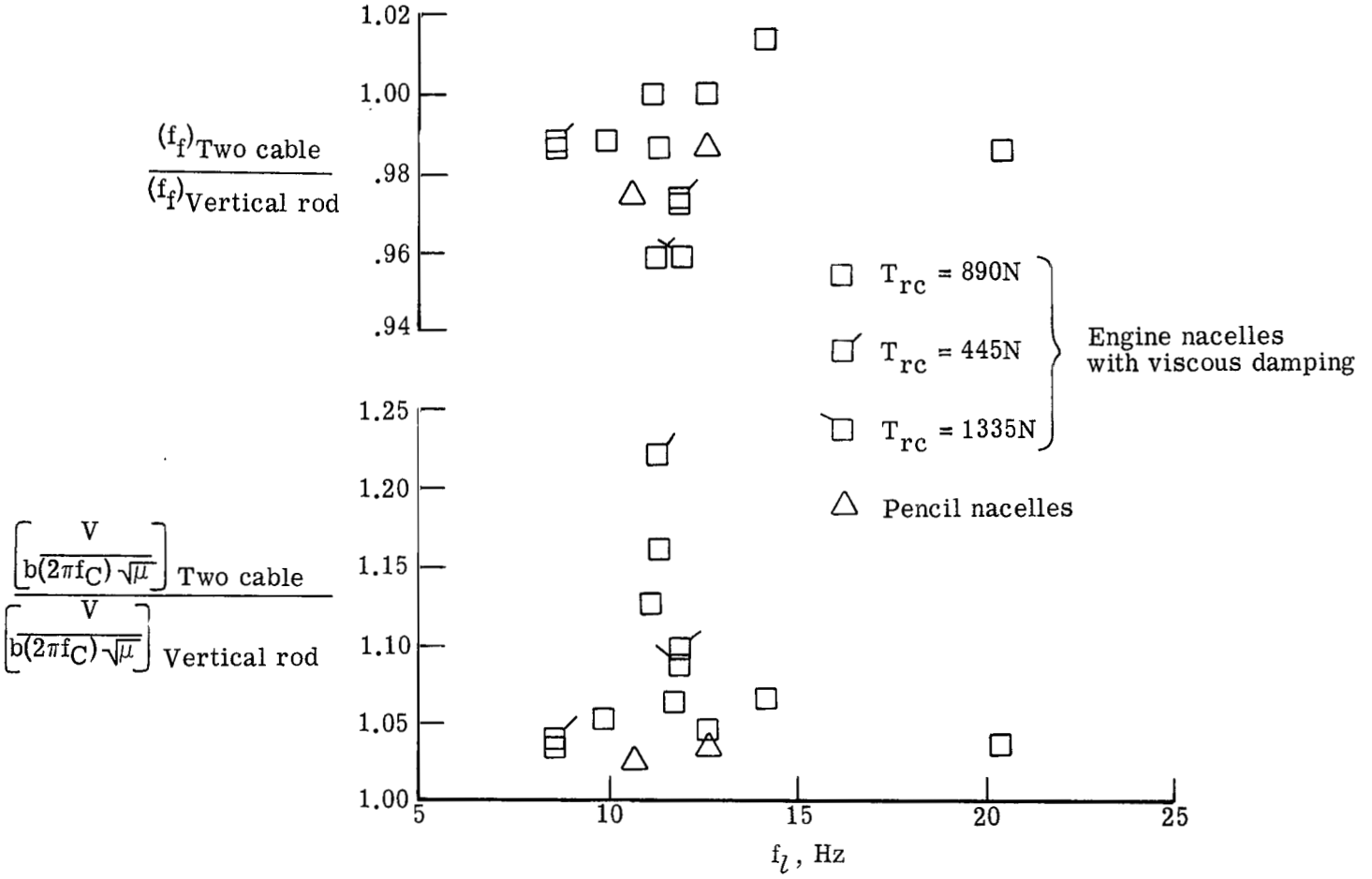

Figure 13.- Comparison of TDT data for the two mount systems, including effects of varying two-cable-mount stiffness.

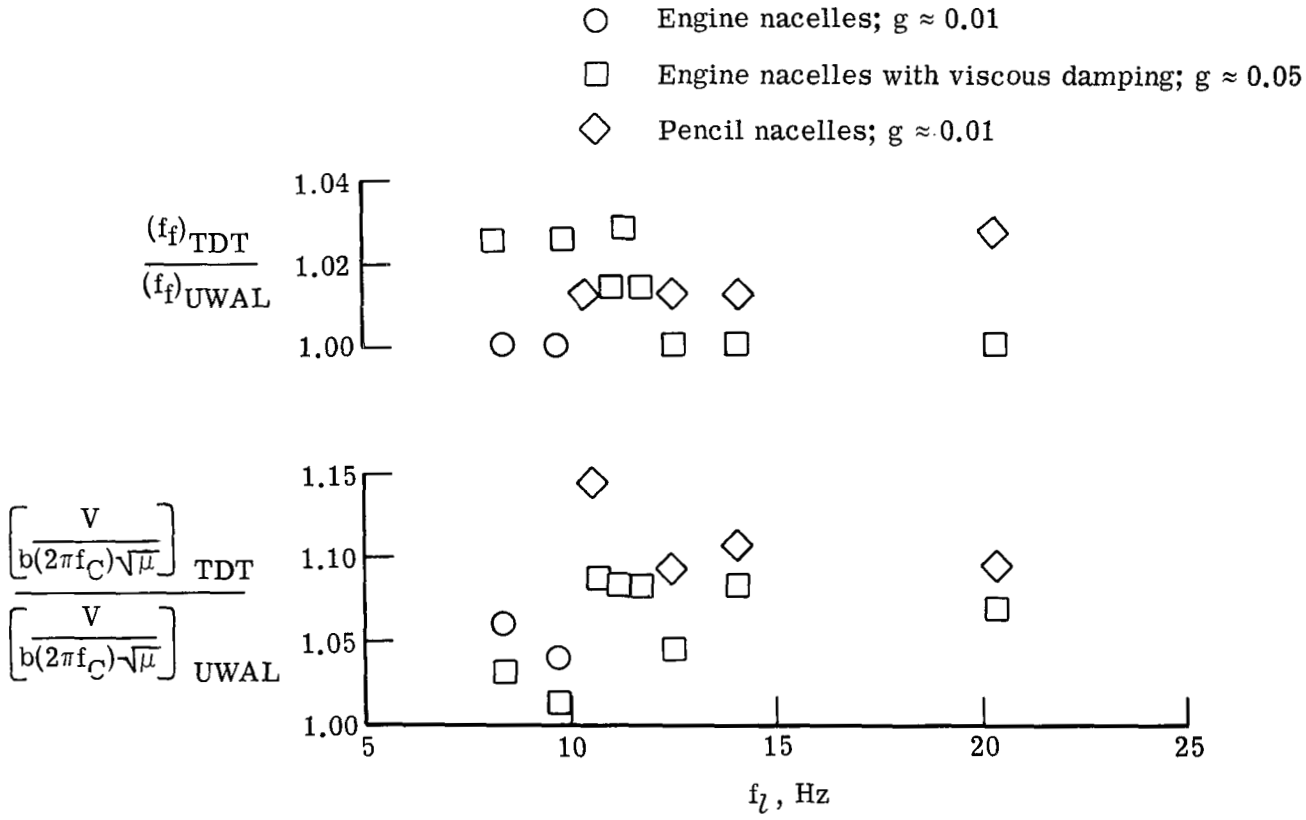

Figure 14.- Comparison of vertical-rod-mount data for the two wind tunnels.

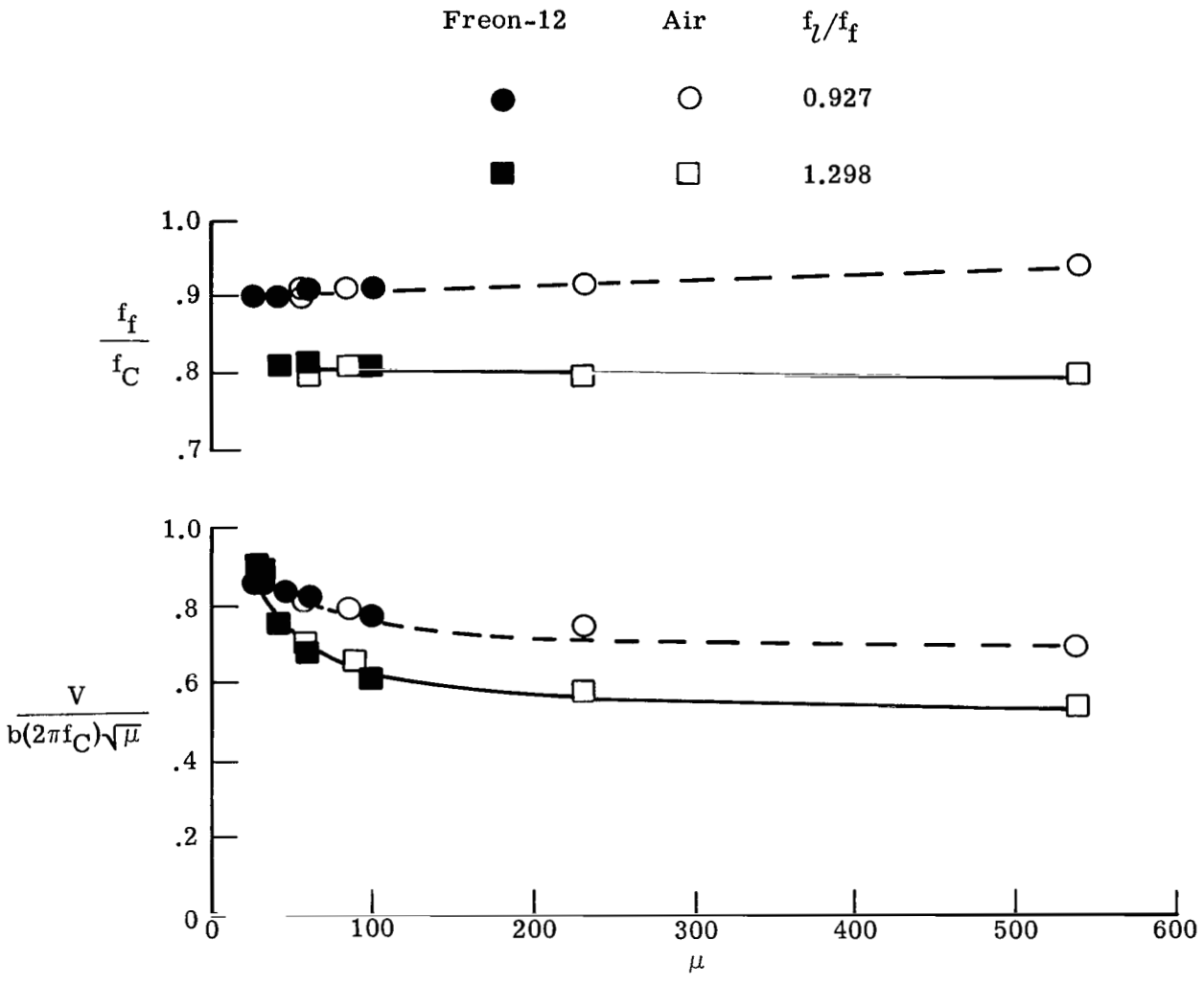

Figure 15.- Effects of mass ratio as determined in the TDT on vertical rod mount. Engine nacelles; $g \approx 0.01$.

"The aeronautical and space activities of the United States shall be conducted so as to contribute . . . to the expansion of human knowledge of phenomena in the atmosphere and space. The Administration shall provide for the widest practicable and appropriate dissemination of information concerning its activities and the results thereof."

—NATIONAL AERONAUTICS AND SPACE ACT OF 1958

NASA SCIENTIFIC AND TECHNICAL PUBLICATIONS

TECHNICAL REPORTS: Scientific and technical information considered important, complete, and a lasting contribution to existing knowledge.

TECHNICAL NOTES: Information less broad in scope but nevertheless of importance as a contribution to existing knowledge.

TECHNICAL MEMORANDUMS: Information receiving limited distribution because of preliminary data, security classification, or other reasons.

CONTRACTOR REPORTS: Scientific and technical information generated under a NASA contract or grant and considered an important contribution to existing knowledge.

TECHNICAL TRANSLATIONS: Information published in a foreign language considered to merit NASA distribution in English.

SPECIAL PUBLICATIONS: Information derived from or of value to NASA activities. Publications include conference proceedings, monographs, data compilations, handbooks, sourcebooks, and special bibliographies.

TECHNOLOGY UTILIZATION PUBLICATIONS: Information on technology used by NASA that may be of particular interest in commercial and other non-aerospace applications. Publications include Tech Briefs, Technology Utilization Reports and Notes, and Technology Surveys.

Details on the availability of these publications may be obtained from:

SCIENTIFIC AND TECHNICAL INFORMATION DIVISION

NATIONAL AERONAUTICS AND SPACE ADMINISTRATION

Washington, D.C. 20546